Mathematical Modelling of a Hydraulic Accumulator for Hydraulic Hybrid Drives

authored by **Andreas Pfeffer, Tobias Glueck, Wolfgang Kemmetmueller, and Andreas Kugi**

and published in *Mathematical and Computer Modelling of Dynamical Systems.*

Cite this article as:

A. Pfeffer, T. Glueck, W. Kemmetmueller, and A. Kugi, "Mathematical modelling of a hydraulic accumulator for hydraulic hybrid drives", *Mathematical and Computer Modelling of Dynamical Systems*, 2016. DOI: 10.1080/13873954.2016.1174716

BibTex entry:

```
% This file was created with JabRef 2.9.2.
% Encoding: Cp1252

@ARTICLE{acinpaper,
  author = {Pfeffer,Andreas and Glueck,Tobias and Kemmetmueller,Wolfgang and
       Kugi,Andreas},
  title = {Mathematical Modelling of a Hydraulic Accumulator for Hydraulic Hybrid
       Drives},
  journal = {Mathematical and Computer Modelling of Dynamical Systems},
  year = {2016},
  doi = {10.1080/13873954.2016.1174716},
  owner = {ap},
  timestamp = {2016.04.05}
}
```

Link to original paper:

http://dx.doi.org/10.1080/13873954.2016.1174716

Contact:

Automation and Control Institute (ACIN)
Vienna University of Technology
Gusshausstrasse 27-29/E376
1040 Vienna, Austria

Internet: www.acin.tuwien.ac.at
E-mail: office@acin.tuwien.ac.at
Phone: +43 1 58801 37601
Fax: +43 1 58801 37699

To appear in *Mathematical and Computer Modelling of Dynamical Systems*
Vol. 00, No. 00, Month 20XX, 1–17

Mathematical Modelling of a Hydraulic Accumulator for Hydraulic Hybrid Drives

A. Pfeffer*, T. Glück, W. Kemmetmüller, and A. Kugi

Automation and Control Institute, TU Wien, Vienna, Austria;

(*released November 2015*)

Hydraulic accumulators are used as energy storages in a wide area of applications. In particular in automotive hybrid drive-trains this type of energy storage is an interesting alternative to today's common strategies like chemical batteries or flywheels. This paper deals with the mathematical modelling of a hydraulic accumulator for passenger vehicles, which comprises a carbon fibre reinforced plastics (CFRP) body and aluminium piston. The thermodynamical behaviour of the oil and gas as well as the interaction with the CFRP body is investigated in detail. Starting from a complex model, two models of reduced complexity are derived. The validation of these models with measurement data from a test drive with a prototype series hydraulic hybrid drive-train proves their high accuracy.

Keywords: Hybrid Powertrain; Hydraulic Accumulator; Hydraulic Hybrid Drive; Heat Transfer; Fluidic Systems

AMS Subject Classification: 93A05;80A05;80A20;76N15;65H10;

1. Introduction

To comply with future exhaust emission standards, the automotive industry is developing alternative fuel saving strategies besides the common downsizing and turbo-charging concepts [1]. In the last two decades, hybrid drives became more and more popular, see, e.g., [2–4]. The most commonly used hybrid concept in passenger vehicles combines a combustion engine with an electric machine and a rechargeable battery as an energy storage. From an economic perspective, the main disadvantage of this concept is the high price of the batteries [5, 6]. Another hybrid drive strategy uses a hydrostatic drive in combination with a hydraulic accumulator for recuperating the braking energy [7–10, 10–15]. Using a hydraulic accumulator as an energy storage device is a well established concept also in many other technical fields of application, see, e.g., [5, 16–21]. The benefits of hydraulic accumulators over batteries are their lower price, the ability of combining high power in- and outputs with a high charge and discharge frequency [10, 22], and their higher power density [5]. The economical usage of the stored energy requires an intelligent control strategy and the accurate information about the actual powers flows and the stored energy. For batteries, the voltage indicates the so-called state of charge (SOC)[10]. Determining the state of charge for a hydraulic accumulator requires the knowledge of the actual amount of oil stored in the hydraulic accumulator [22–25]. The oil volume is directly related to the energy stored in

*Corresponding author. Email: pfeffer@acin.tuwien.ac.at

the gas volume [15, 22]. For piston type accumulators, a direct measurement of the oil volume is possible using a displacement sensor. This method is, however, technically difficult and costly and, therefore, not attractive for automotive applications. Furthermore, a direct volume measurement is not applicable to bladder type accumulators. Thus, estimation strategies using only standard pressure and temperature sensors are preferred in practical applications, see, e.g., [26]. For the development and the evaluation of such SOC estimation strategies, tailored mathematical models are necessary. These models are also useful for the evaluation of the overall hydraulic hybrid drive system, mainly, because real test drives are expensive and time consuming. Thus, this paper is devoted to the development and the experimental validation of a mathematical model for a piston type hydraulic accumulator. Therein, special emphasis is given to the influence of the ambient, gas and oil temperature as well as the large variations in the gas pressure.

Most of the works presented in literature that are concerned with the modelling of hydraulic accumulators focus on the modelling of the gas behaviour, cf. [7, 8, 14, 19, 27–29]. In many cases the gas volume is filled with a foam to affect the thermal capacity [7, 8, 30]. This allows to model the thermal behaviour of the gas volume with a constant thermal time constant. In the present case, there is no filling material used in the accumulator, which is why the thermal behaviour of nitrogen has to be taken into account in a wide pressure range. For an accurate estimation of the SOC, the mathematical model also has to account for the interaction with the ambience, since the ambient temperature may vary from $-40\,^{\circ}\mathrm{C}$ up to $60\,^{\circ}\mathrm{C}$.

The hydraulic accumulator under consideration features a carbon fibre reinforced plastic (CFRP) housing, which has quite different characteristics compared to the steel housing used in classical accumulators typically considered in literature. Due to these facts, the models proposed in literature cannot be directly applied to the considered accumulator. Thus, there is a need for a mathematical model tailored to this type of accumulator.

The paper is organised as follows: in Section 2, the mathematical model of the hydraulic piston accumulator is presented, where models of different levels of detail and complexity are discussed. These mathematical models are validated by measurement results of the real system in Section 3. The paper closes with a short summary and an outlook to future research activities.

2. Mathematical Model

A schematic of the hydraulic piston accumulator is shown in Figure 1. The housing consists of the CFRP pipe and two aluminium sealing ends. A moveable aluminium piston sealed by a gasket separates the gas chamber from the oil chamber.

The gas chamber is pre-charged with nitrogen. During the braking phases of the hybrid car, the hydraulic drive pumps oil into the oil chamber of the accumulator. The piston then moves to the left and thus compresses the gas. The following mathematical model is based on a detailed analysis of the heat fluxes between the solid and fluid (gas) parts of the accumulator and the influence of the mass flow of oil entering the oil chamber. The next section describes the modelling of the aluminium parts of the accumulator, i.e., the piston and the two sealing ends.

Post-print version of the article: A. Pfeffer, T. Glueck, W. Kemmetmueller, and A. Kugi, "Mathematical modelling of a hydraulic accumulator for hydraulic hybrid drives", *Mathematical and Computer Modelling of Dynamical Systems*, 2016. DOI: 10.1080/13873954.2016.1174716
The content of this post-print version is identical to the published paper but without the publisher's final layout or copy editing.

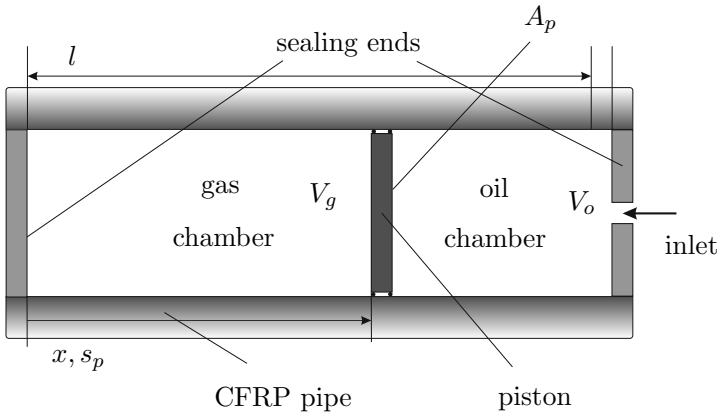

Figure 1. Schematic of the hydraulic piston accumulator.

2.1. *Piston and sealing end*

Due to the high heat conductance of aluminium, a homogeneous temperature can be assumed in the piston and the sealing end. The balance of energy for the piston (index p) yields

$$\frac{\mathrm{d}T_p}{\mathrm{d}t} = \frac{\dot{Q}_{g,p} + \dot{Q}_{o,p}}{m_p c_{al}}, \tag{1}$$

with the piston temperature T_p, the constant specific heat capacity of aluminium c_{al}, the mass m_p of the piston, and the heat flux from the gas to the piston $\dot{Q}_{g,p}$ and from the oil to the piston $\dot{Q}_{o,p}$, respectively. These heat fluxes result from Newton's law of cooling [31], in the form

$$\dot{Q}_{g,p} = \alpha_{g,p} A_p (T_g - T_p) \tag{2a}$$

$$\dot{Q}_{o,p} = \alpha_{o,p} A_p (T_o - T_p). \tag{2b}$$

Herein, $\alpha_{g,p}$ and $\alpha_{o,p}$ denote the constant heat transfer coefficients from gas to the piston and from oil to the piston, respectively, A_p is the effective piston area, T_g the gas temperature and T_o the oil temperature. For the mathematical model, only the sealing end on the gas side is of interest, because the oil temperature is assumed to be known and thus no model for the temperature in the oil chamber is required. Analogous to the piston, the temperature differential equation for the sealing end on the gas side result in

$$\frac{\mathrm{d}T_e}{\mathrm{d}t} = \frac{\dot{Q}_{g,e} + \dot{Q}_{a,e}}{m_e c_{al}}, \tag{3}$$

with the mass m_e of the sealing end. The heat fluxes from the sealing end to the gas $\dot{Q}_{g,e}$ and from the ambiance to the sealing end $\dot{Q}_{a,e}$ read as

$$\dot{Q}_{g,e} = \alpha_{g,e} A_e (T_g - T_e) \tag{4a}$$

$$\dot{Q}_{a,e} = \alpha_{a,e} A_e (T_a - T_e), \tag{4b}$$

Post-print version of the article: A. Pfeffer, T. Glueck, W. Kemmetmueller, and A. Kugi, "Mathematical modelling of a hydraulic accumulator for hydraulic hybrid drives", *Mathematical and Computer Modelling of Dynamical Systems*, 2016. DOI: 10.1080/13873954.2016.1174716
The content of this post-print version is identical to the published paper but without the publisher's final layout or copy editing.

with the corresponding constant heat transfer coefficients $\alpha_{g,e}$ and $\alpha_{a,e}$, the effective area A_e and the ambient temperature T_a, cf. (2).

2.2. *Carbon fibre (CFRP) pipe*

Because of the low heat conductance of the CFRP material and the layered structure in radial direction, the temperature distribution is inhomogeneous in the CFRP pipe. The wall thickness of the CFRP pipe is more than 8 times smaller than the diameter of the pipe, which allows to approximately describe the pipe in Cartesian coordinates (x, y, z), see Figure 2. The heat diffusion equation is given by [31]

$$\rho_c c_c \frac{\mathrm{d}T_c}{\mathrm{d}t} = \frac{\partial}{\partial x}\left(\lambda_x \frac{\partial T_c}{\partial x}\right) + \frac{\partial}{\partial y}\left(\lambda_y \frac{\partial T_c}{\partial y}\right) + \frac{\partial}{\partial z}\left(\lambda_z \frac{\partial T_c}{\partial z}\right), \tag{5}$$

with the density ρ_c, the heat capacity c_c, the temperature T_c and the heat conductances λ_i, $i = \{x, y, z\}$ of the CFRP material. Using the symmetry boundary condition in circumferential direction (z-direction), the temperature T_c is independent of z, i.e., $T_c = T_c(x, y, t)$. Moreover, by neglecting the heat conduction in longitudinal x-direction due to the small cross section of the pipe, (5) becomes

$$\rho_c c_c \frac{\mathrm{d}T_c(x, y, t)}{\mathrm{d}t} = \lambda_y \frac{\partial^2 T_c(x, y, t)}{\partial y^2}, \tag{6}$$

with the constant heat conductance λ_y in radial y-direction. For the outer surface $y = r_{os}$, the boundary condition for the CFRP pipe reads as

$$\lambda_y \left.\frac{\partial T_c(x, y, t)}{\partial y}\right|_{y=r_{os}} = \dot{q}_{a,c} = \alpha_{a,c}\left(T_a(t) - T_c(x, r_{os}, t)\right), \tag{7}$$

with the heat flux density $\dot{q}_{a,c}$ from the ambiance to the CFRP pipe and the corresponding heat transfer coefficient $\alpha_{a,c}$, see, e.g., [31]. The inner surface $y = r_{is}$ of the CFRP pipe is either in contact with oil or with nitrogen depending on the piston position s_p. The boundary condition can be formulated as

$$\lambda_y \left.\frac{\partial T_c(x, y, t)}{\partial y}\right|_{y=r_{is}} = \dot{q}_{g,c} + \dot{q}_{o,c}, \tag{8}$$

with the heat flux density $\dot{q}_{g,c}$ from the gas to the CFRP pipe

$$\dot{q}_{g,c} = \alpha_{g,c}(1 - \sigma(x - s_p))\left(T_c(x, r_{is}, t) - T_g(t)\right), \tag{9a}$$

and the heat flux density $\dot{q}_{o,c}$ from the oil to the CFRP pipe

$$\dot{q}_{o,c} = \alpha_{o,c}\sigma(x - s_p)\left(T_c(x, r_{is}, t) - T_o(t)\right). \tag{9b}$$

Here, $\alpha_{g,c}$ and $\alpha_{o,c}$ are the corresponding constant heat transfer coefficients. Moreover, σ denotes the Heaviside function, which is used to represent the influence of the piston position on the coupling of the wall with the fluids, see Figure 2.

Post-print version of the article: A. Pfeffer, T. Glueck, W. Kemmetmueller, and A. Kugi, "Mathematical modelling of a hydraulic accumulator for hydraulic hybrid drives", *Mathematical and Computer Modelling of Dynamical Systems*, 2016. DOI: 10.1080/13873954.2016.1174716
The content of this post-print version is identical to the published paper but without the publisher's final layout or copy editing.

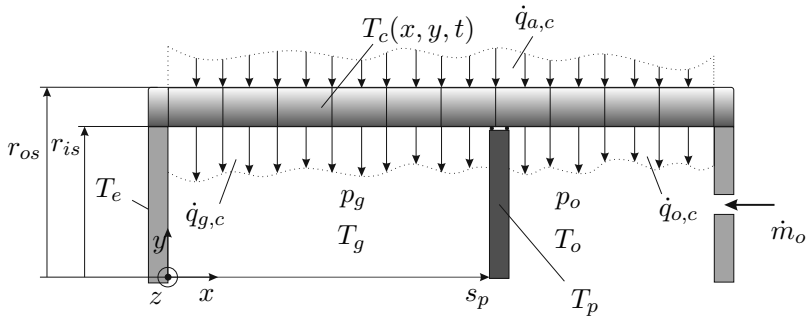

Figure 2. Detailed schematic of the accumulator with the main heat fluxes of the CFRP pipe.

For simulation studies the partial differential equation (PDE) (6) with the boundary conditions (7) and (8) must be approximated by a set of ordinary differential equations (ODE). In this work, three approaches for the approximation of the PDE are examined:

(1) In the detailed model (*Model I*), a temperature gradient in both x- and y-direction is taken into account.
(2) For the second model (*Model II*), a constant temperature in y-direction is presumed, whereas the temperature gradient in x-direction is still considered.
(3) In the simplest third model (*Model III*), a homogeneous temperature for the whole CFRP pipe is considered.

The influence of these simplifications on the model accuracy is analysed in Section 3.

2.2.1. CFRP-Model I

In a first step, the y-direction is discretised with n_y elements and by using the central difference quotient on the right-hand side of (6), we get

$$\frac{\mathrm{d}T_{c,i}(x,t)}{\mathrm{d}t} = \frac{\lambda_y}{\rho_c c_c}\left(\frac{T_{c,i+1}(x,t) - 2T_{c,i}(x,t) + T_{c,i-1}(x,t)}{d_y^2}\right), \quad i = 1,\dots,n_y, \tag{10}$$

where the second index i of the temperature $T_{c,i}$ identifies the discretisation point at $y = id_y$, $i = 0,\dots,n_y$ with the discretisation step length $d_y = (r_{os} - r_{is})/(n_y - 1)$. The temperatures $T_{c,0}$ and T_{c,n_y+1}, which arise in (10), can be eliminated by discretising the boundary conditions (7) and (8) in the form

$$\left.\frac{\partial T_c(x,y,t)}{\partial y}\right|_{y=r_{is}} = \frac{T_{c,2}(x,t) - T_{c,0}(x,t)}{2d_y} = \frac{\alpha_{g,c}}{\lambda_y}(1-\sigma(x-s_p))\big(T_{c,1}(x,t) - T_g(t)\big) + \frac{\alpha_{o,c}}{\lambda_y}\sigma(x-s_p)\big(T_{c,1}(x,t) - T_o(t)\big) \tag{11a}$$

$$\left.\frac{\partial T_c(x,y,t)}{\partial y}\right|_{y=r_{os}} = \frac{T_{c,n_y+1}(x,t) - T_{c,n_y-1}(x,t)}{2d_y} = \frac{\alpha_{a,c}}{\lambda_y}\big(T_a(t) - T_{c,n_y}(x,t)\big). \tag{11b}$$

Post-print version of the article: A. Pfeffer, T. Glueck, W. Kemmetmueller, and A. Kugi, "Mathematical modelling of a hydraulic accumulator for hydraulic hybrid drives", *Mathematical and Computer Modelling of Dynamical Systems*, 2016. DOI: 10.1080/13873954.2016.1174716
The content of this post-print version is identical to the published paper but without the publisher's final layout or copy editing.

Inserting $T_{c,0}(x,t)$ and $T_{c,n_y+1}(x,t)$ from (11) into (10) results in the boundary temperature ODEs

$$\frac{\mathrm{d}T_{c,1}(x,t)}{\mathrm{d}t} = \frac{2}{\rho_c c_c}\left(\lambda_y \frac{T_{c,2}(x,t)-T_{c,1}(x,t)}{d_y^2} - \frac{\alpha_{g,c}}{d_y}\big(1-\sigma(x-s_p)\big)\big(T_{c,1}(x,t)-T_g(t)\big) - \frac{\alpha_{o,c}}{d_y}\sigma(x-s_p)\big(T_{c,1}(x,t)-T_o(t)\big)\right) \tag{12a}$$

$$\frac{\mathrm{d}T_{c,n_y}(x,t)}{\mathrm{d}t} = \frac{2}{\rho_c c_c}\left(\lambda_y \frac{T_{c,n_y-1}(x,t)-T_{c,n_y}(x,t)}{d_y^2} - \frac{\alpha_{a,c}}{d_y}\big(T_{c,n_y}(x,t)-T_a(t)\big)\right). \tag{12b}$$

The ODEs for the interior temperatures $i = 2,\dots,n_y-1$ are given by (10). The resulting set of differential equations is defined as a function of the scalar variable $x \in [0,l]$. To balance the heat fluxes through the pipe to the ambience, the gas and the oil, the heat flux densities $\dot{q}_{a,c}(t)$, $\dot{q}_{g,c}(t)$ and $\dot{q}_{o,c}(t)$ are integrated over the corresponding surface

$$\dot{Q}_{g,c} = \int_{A_g(s_p)} \dot{q}_{g,c}\mathrm{d}A = \alpha_{g,c} 2\pi r_{is} \int_0^{s_p} T_{c,1}(x,t) - T_g(t)\mathrm{d}x, \tag{13a}$$

$$\dot{Q}_{o,c} = \int_{A_o(s_p)} \dot{q}_{o,c} = \alpha_{o,c} 2\pi r_{is} \int_{s_p}^{l} T_{c,1}(x,t) - T_o(t)\mathrm{d}x, \tag{13b}$$

$$\dot{Q}_{a,c} = \int_{A_a} \dot{q}_{a,c} = -\alpha_{a,c} 2\pi r_{os} \int_0^{l} T_{c,n_y}(x,t) - T_a(t)\mathrm{d}x. \tag{13c}$$

To calculate these integrals, a discretisation in n_x elements along the x-direction is utilised. Figure 3 shows a schematic of the discretisation in x- and y-direction for the *Model I*. The mean temperature $\bar{T}_{c,i,j}$ of the i-th discretisation point in

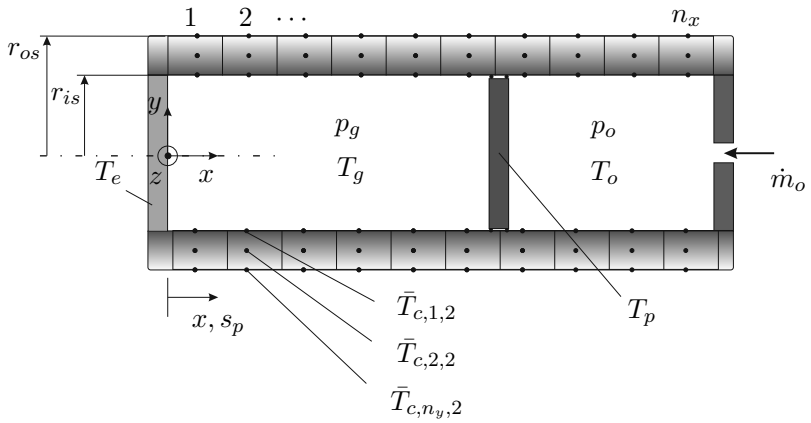

Figure 3. Detailed schematic of the accumulator with the discretisation of the CFRP pipe of *Model I*, with $n_x = 10$ and $n_y = 3$.

Post-print version of the article: A. Pfeffer, T. Glueck, W. Kemmetmueller, and A. Kugi, "Mathematical modelling of a hydraulic accumulator for hydraulic hybrid drives", *Mathematical and Computer Modelling of Dynamical Systems*, 2016. DOI: 10.1080/13873954.2016.1174716
The content of this post-print version is identical to the published paper but without the publisher's final layout or copy editing.

y-direction and the j-th volume in x-direction is defined by

$$\bar{T}_{c,i,j}(t) = \frac{1}{d_x} \int_{(j-1)d_x}^{jd_x} T_{c,i}(x,t)\mathrm{d}x, \quad i = 1,\dots,n_y,\ j = 1,\dots,n_x. \tag{14}$$

Applying the approximation $T_{c,i}(x,t)\big|_{(j-1)d_x \le x \le jd_x} \approx \bar{T}_{c,i,j}$, (13a) results in

$$\dot{Q}_{g,c} = \sum_{j=1}^{n_x} \dot{Q}_{g,c,j} \tag{15}$$

with

$$\dot{Q}_{g,c,j} = \alpha_{g,c} 2\pi r_{is} \left(\bar{T}_{c,1,j}(t) - T_g(t)\right) d_x \left(1 - \xi_j(s_p)\right) \tag{16}$$

and

$$\xi_j(s_p) = \begin{cases} 0 & s_p > (j+1)d_x \\ \left(1 - \frac{s_p - jd_x}{d_x}\right) & jd_x \le s_p \le (j+1)d_x \\ 1 & s_p < jd_x \end{cases}. \tag{17}$$

The heat fluxes $\dot{Q}_{o,c,j}$ and $\dot{Q}_{a,c,j}$ can be calculated in an analogous way

$$\dot{Q}_{o,c,j} = \alpha_{o,c} 2\pi r_{is} \left(\bar{T}_{c,1,j}(t) - T_o(t)\right) \xi_j(s_p) d_x, \tag{18a}$$

$$\dot{Q}_{a,c,j} = -\alpha_{a,c} 2\pi r_{os} \left(\bar{T}_{c,n_y,j}(t) - T_a(t)\right) d_x. \tag{18b}$$

This yields the discretised ODEs (10) and (12) in the form

$$\frac{\mathrm{d}\bar{T}_{c,1,j}(t)}{\mathrm{d}t} = \frac{2}{\rho_c c_c} \left(\lambda_y \frac{\bar{T}_{c,2,j}(t) - \bar{T}_{c,1,j}(t)}{d_y^2} - \frac{1}{d_y} \frac{1}{2\pi r_{is} d_x} \left(\dot{Q}_{g,c,j} + \dot{Q}_{o,c,j} \right) \right) \tag{19a}$$

$$\frac{\mathrm{d}\bar{T}_{c,i,j}(t)}{\mathrm{d}t} = \frac{\lambda_y}{\rho_c c_c} \left(\frac{\bar{T}_{c,i+1}(x,t) - 2\bar{T}_{c,i}(x,t) + \bar{T}_{c,i-1}(x,t)}{d_y^2} \right), \quad i = 2,\dots,n_y - 1 \tag{19b}$$

$$\frac{\mathrm{d}\bar{T}_{c,n_y,j}(t)}{\mathrm{d}t} = \frac{2}{\rho_c c_c} \left(\lambda_y \frac{\bar{T}_{c,n_y-1,j}(t) - \bar{T}_{c,n_y,j}(t)}{d_y^2} + \frac{1}{d_y} \frac{1}{2\pi r_{os} d_x} \dot{Q}_{a,c,j} \right), \tag{19c}$$

with $j = 1,\dots,n_x$. The influence of the number of discretisation elements n_x and n_y on the model accuracy will be discussed in Section 3.

2.2.2. CFRP-Model II and III

Model I exhibits a rather large complexity, in particular, if a large number n_x and n_y of discretisation elements is used. Thus, this model might be well suited for simulation purposes but not for a model-based controller design. In order to derive simplified models, first the temperature gradient in y-direction is neglected, which may be justified by the small thickness of the CFRP material. This model will be

Post-print version of the article: A. Pfeffer, T. Glueck, W. Kemmetmueller, and A. Kugi, "Mathematical modelling of a hydraulic accumulator for hydraulic hybrid drives", *Mathematical and Computer Modelling of Dynamical Systems*, 2016. DOI: 10.1080/13873954.2016.1174716
The content of this post-print version is identical to the published paper but without the publisher's final layout or copy editing.

referred to as (*Model II*). The resulting equations can be easily derived in the form

$$\frac{\mathrm{d}\bar{T}_{c,m,j}(t)}{\mathrm{d}t} = \frac{-1}{\rho_c c_c (r_{os}-r_{is})^2 \pi d_x} \left(\dot{Q}_{g,c,j} + \dot{Q}_{o,c,j} - \dot{Q}_{a,c,j}\right), \quad j = 1, \ldots, n_x. \tag{20}$$

Finally, in the most simple *Model III* a homogeneous temperature also in x-direction is assumed, i.e., the whole CFRP pipe is described by one single temperature $\bar{T}_c$. This assumption is frequently applied in literature to the modelling of accumulators and, as will be discussed later, yields to a rather coarse approximation of the real behaviour. Nevertheless, this model can still be useful for a controller design. The temperature $\bar{T}_c$ is then described by the ODE

$$\begin{aligned}\frac{\mathrm{d}\bar{T}_c(t)}{\mathrm{d}t} = \frac{-1}{\rho_c c_c (r_{os}-r_{is})^2 \pi l} &\left(\alpha_{g,c} A_g \left(\bar{T}_c(t) - T_g(t)\right) + \alpha_{o,c} A_o \left(\bar{T}_c(t) - T_o(t)\right)\right. \\ &\left. + \alpha_{a,c} A_a \left(\bar{T}_c(t) - T_a(t)\right)\right),\end{aligned} \tag{21}$$

with the effective surfaces $A_g = 2\pi r_{is} s_p$, $A_o = 2\pi r_{is}(l - s_p)$ and $A_a = 2\pi r_{os} l$.

2.3. *Gas chamber*

The application of the accumulator in an automotive system brings along a large variation of the ambient (and thus gas) temperature in the range from $-20\,^{\circ}\mathrm{C}$ up to $60\,^{\circ}\mathrm{C}$. Furthermore, the gas pressure varies from the pre-charge pressure of 120 bar to approximately 350 bar when the accumulator is completely filled. To accurately describe the behaviour of the gas (nitrogen) in the entire operating range, the algebraic real gas equation in the form

$$p_g V_g = m_g R_s T_g z \tag{22}$$

is utilised, see, e.g., [32, 33]. Therein, both the gas pressure p_g and the gas temperature T_g are assumed to be homogeneous in the entire gas chamber. Even if a homogeneous gas temperature might be a considerable simplification of reality, it is almost impossible to derive a reasonable model of the temperature distribution in the gas chamber. The measurement results of Section 3, however, confirm that the influence of this simplification on the model accuracy is quite small and thus feasible. The gas volume $V_g = A_p s_p + V_{g,0}$, with the dead volume of the gas side $V_{g,0}$, is a function of the piston position and thus of the SOC of the accumulator. The specific behaviour of nitrogen is described by the specific gas constant R_s and the compressibility factor $z = z(p_g, T_g)$, which can be found in the literature, see, e.g., [32, 34, 35]. Due to the sealed piston and the gas-tight housing, the gas mass can be assumed to be constant $\rho_g V_g = m_g = \text{const.}$, where $\rho_g = \rho_g(p_g, T_g)$ denotes the gas mass density. The mass balance gives

$$\frac{\mathrm{d}}{\mathrm{d}t}\left(\rho_g(p_g, T_g) V_g\right) = 0. \tag{23}$$

The balance of energy for the gas chamber can be written in the form, see, e.g., [32],

$$\frac{\mathrm{d}H_g}{\mathrm{d}t} = \dot{Q}_g + \dot{W}_g + \frac{\mathrm{d}(p_g V_g)}{\mathrm{d}t}, \tag{24}$$

Post-print version of the article: A. Pfeffer, T. Glueck, W. Kemmetmueller, and A. Kugi, "Mathematical modelling of a hydraulic accumulator for hydraulic hybrid drives", *Mathematical and Computer Modelling of Dynamical Systems*, 2016. DOI: 10.1080/13873954.2016.1174716
The content of this post-print version is identical to the published paper but without the publisher's final layout or copy editing.

with the enthalpy H_g, the overall heat flux $\dot{Q}_g$ and the shaft work $\dot{W}_g = -p_g \dot{V}_g$. With the isobaric coefficient of thermal expansion $\beta = \beta(p_g, T_g)$, see, e.g., [33],

$$\beta(p_g, T_g) = -\frac{1}{\rho_g}\left(\frac{\partial \rho_g}{\partial T_g}\right)_p, \tag{25}$$

the specific enthalpy h_g can be written in the form

$$\frac{\mathrm{d}h_g}{\mathrm{d}t} = c_p(p_g, T_g)\frac{\mathrm{d}T_g}{\mathrm{d}t} + \frac{1}{\rho_g}\left(1 - \beta(p_g, T_g)T_g\right)\frac{\mathrm{d}p_g}{\mathrm{d}t}, \tag{26}$$

where $c_p = c_p(p_g, T_g)$ denotes the isobaric heat capacity. The coefficients $\rho(p_g, T_g), z(p_g, T_g), c_p(p_g, T_g)$ and $\beta(p_g, T_g)$ are tabulated in literature, see [36]. Combining (22), (23), (24) and (26) gives, after a short calculation, the ODE for the gas pressure

$$\frac{\mathrm{d}p_g}{\mathrm{d}t} = -\frac{R_s T_g z}{N_g}\frac{\partial \rho_g}{\partial T_g}\left(\dot{Q}_{g,c} + \dot{Q}_{g,p} + \dot{Q}_{g,e}\right) - \frac{\rho_g c_p p_g}{N_g}\frac{\mathrm{d}V_g}{\mathrm{d}t} \tag{27}$$

with

$$N_g = N_g(p_g, T_g) = V_g\left(p_g c_p \frac{\partial \rho_g}{\partial p_g} + R_s T_g^2 z \beta \frac{\partial \rho_g}{\partial T_g}\right). \tag{28}$$

The heat flux from the gas to the piston $\dot{Q}_{g,p}$ is given by (2a) and the heat flux from the gas to the sealing end $\dot{Q}_{g,e}$ results from (4a). The heat flux from the gas to the CFRP pipe $\dot{Q}_{g,c}$ follows from (15) and (16) for the *Model I* and *Model II*, and is given by

$$\dot{Q}_{g,c} = \alpha_{g,c} A_g (\bar{T}_c - T_g) \tag{29}$$

for *Model III*, cf. (21).

2.4. *Oil chamber*

The compressibility of oil is much lower than that of nitrogen, and is therefore neglected. The oil temperature is accurately measured by a sensor and is kept to an almost constant value due to an oil cooler in the hybrid drive system. Thus, no model for the oil temperature is necessary and the oil density ρ_o can be assumed constant. The mass balance of the oil chamber reads as

$$\frac{\mathrm{d}V_o}{\mathrm{d}t} = -A_p \frac{\mathrm{d}s_p}{\mathrm{d}t} = \frac{\dot{m}_o}{\rho_o}, \tag{30}$$

with the oil volume $V_o = A_p(l - s_p) + V_{o,d}$, the dead volume of the oil side $V_{o,d}$ and the piston surface A_p. Obviously, this entails $\dot{V}_g = -\dot{V}_o = -\dot{m}_o/\rho_o$, where $\dot{m}_o$ denotes the oil mass flow.

Post-print version of the article: A. Pfeffer, T. Glueck, W. Kemmetmueller, and A. Kugi, "Mathematical modelling of a hydraulic accumulator for hydraulic hybrid drives", *Mathematical and Computer Modelling of Dynamical Systems*, 2016. DOI: 10.1080/13873954.2016.1174716
The content of this post-print version is identical to the published paper but without the publisher's final layout or copy editing.

2.5. *Overall model structure*

The presented sub-models can be arranged in form of a semi-explicit differential-algebraic equation

$$\frac{\mathrm{d}}{\mathrm{d}t}\boldsymbol{x} = \boldsymbol{f}(\boldsymbol{x}, T_g, \boldsymbol{T}_\mathrm{c}, \boldsymbol{u}), \quad \boldsymbol{x}(0) = \boldsymbol{x}_0, \tag{31a}$$

$$\frac{\mathrm{d}}{\mathrm{d}t}\boldsymbol{T}_\mathrm{c} = \boldsymbol{f}_\mathrm{c}(\boldsymbol{x}, T_g, \boldsymbol{T}_\mathrm{c}, \boldsymbol{u}), \quad \boldsymbol{T}_c(0) = \boldsymbol{T}_{c_0}, \tag{31b}$$

$$0 = g(s_p, T_g, \dot{m}_o), \tag{31c}$$

with $\boldsymbol{x}^\mathrm{T} = \begin{bmatrix} s_p & p_g & T_p & T_e \end{bmatrix}$ and the vector $\boldsymbol{T}_\mathrm{c}$ which summarizes the temperatures of the CFRP model. Depending on the used CFRP pipe model, the vector $\boldsymbol{T}_\mathrm{c}$ contains $n_x n_y$ states for *Model I* (see (19)), n_x states for *Model II* (see (20)) and a single state for *Model III* (see (21)). The algebraic equation $g(\boldsymbol{x}, T_g, \boldsymbol{u})$ is the real gas equation according to (22) and $\boldsymbol{f}(\boldsymbol{x}, T_g, \boldsymbol{T}_\mathrm{c}, \boldsymbol{u})$ results from (30), (27) with (28), (1) and (3). The input $\boldsymbol{u}$ is given by $\boldsymbol{u}^\mathrm{T} = \begin{bmatrix} \dot{m}_o & T_o & T_a \end{bmatrix}$.

2.6. *Sensor dynamics*

For the model validation the hydraulic accumulator is equipped with

- a pressure sensor for the oil pressure,
- a temperature sensor for the gas temperature,
- a temperature sensor for the ambient temperature,
- a temperature sensor for the surface temperatures of the CFRP pipe, located at the fourth element of *Model I* and *Model II* at the outer surface of the CFRP pipe,
- and a position sensor for the piston position.

In series production hybrid drives, only the pressure sensor, a gas temperature sensor and the standard car ambient temperature sensor are available, see [26].

In order to evaluate the model accuracy, the accuracy and the dynamics of these sensors have to be analysed. This analysis is also important for the design of estimation and control strategies, which only use a subset of the measurement signals of these sensors. Both, the absolute type pressure sensor, mounted on the oil side of the accumulator, and the draw-wire displacement sensor, which is installed at the sealing end on the gas side, are prototypes. They exhibit a rise time of approximately 800 µs, which is small compared to the systems dynamics and thus negligible. The accuracy of the pressure and position sensor is 1 %FS and 0.5 %FS, respectively. These measurements can be considered as ideal. Moreover, the friction in the piston is low such that the gas pressure is basically equal to the measured oil pressure. The dynamics of the temperature sensors is strongly related to their heat capacity and the heat transfer coefficients. To measure the ambient and the surface temperature, T-type class 1 sheat-thermocouples [37] with a rise time of approximately 150 ms and an accuracy of ±0.5 °C are used. These types of sensors exhibit a fast dynamics due to their low heat capacity and high heat transfer coefficients and thus can also be considered ideal. The used NTC-type gas temperature sensor [38] shows a rise time of approximately 3.5 s and a worst case accuracy of 19.5 % at −40 °C.

Post-print version of the article: A. Pfeffer, T. Glueck, W. Kemmetmueller, and A. Kugi, "Mathematical modelling of a hydraulic accumulator for hydraulic hybrid drives", *Mathematical and Computer Modelling of Dynamical Systems*, 2016. DOI: 10.1080/13873954.2016.1174716
The content of this post-print version is identical to the published paper but without the publisher's final layout or copy editing.

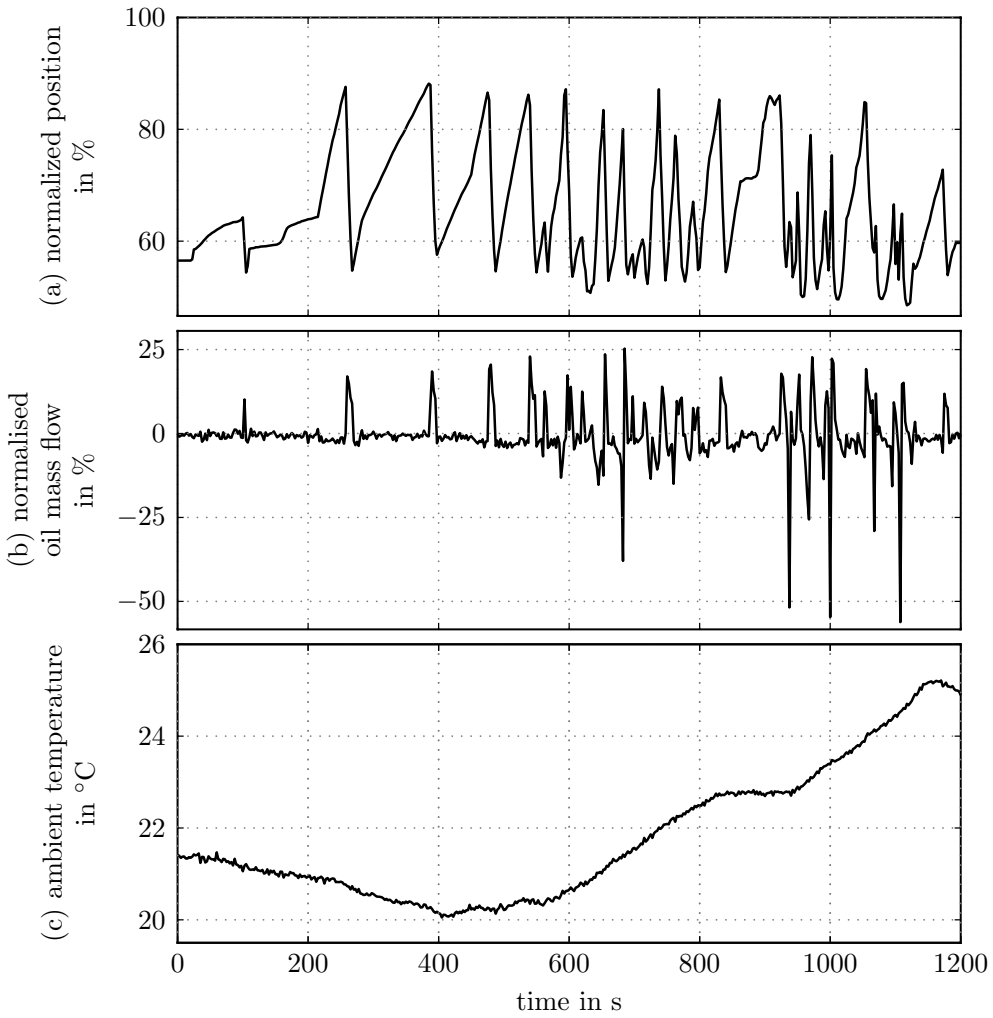

Figure 4. Plot of the measured model inputs over time: (a) normalised measured piston position $s_{p,\mathrm{m}}$; (b) normalised measured oil mass flow $\dot{m}_{o,\mathrm{m}}$; (c) measured ambient temperature $T_{a,\mathrm{m}}$.

3. Model validation

Simulation results are compared to measurement data to evaluate the accuracy of the developed models. The measurement data is obtained from a road test drive on a test track by a hybrid hydraulic car. The considered prototype of the hydraulic piston-type accumulator is installed in a series hydraulic hybrid system. The measured model inputs, i.e., the oil mass flow $\dot{m}_{o,m}$ with the corresponding piston position $s_{p,m}$, and the ambient temperature $T_{a,m}$, are depicted in Figure 4. Here, the piston position is normalised to the maximum piston stroke and the oil mass flow is normalised to the maximum flow of the connected hydrostatic drive. Please note that the index m always refers to the corresponding measured quantities. The oil temperature is approximatively constant at $T_{o,m} \approx 22\,^{\circ}\mathrm{C}$. The piston position $s_{p,m}$ shows the repeated filling and emptying of the hydraulic accumulator, where the speed of this process varies depending on the actual driving situation. In contrast, the ambient and the oil temperature change only slowly which confirms the assumptions made in Section 2.

For the simulation studies, a suitable choice of the number of elements n_x and n_y has to be found for *Model I* and *Model II*. Simulation studies indicate that

Post-print version of the article: A. Pfeffer, T. Glueck, W. Kemmetmueller, and A. Kugi, "Mathematical modelling of a hydraulic accumulator for hydraulic hybrid drives", *Mathematical and Computer Modelling of Dynamical Systems*, 2016. DOI: 10.1080/13873954.2016.1174716
The content of this post-print version is identical to the published paper but without the publisher's final layout or copy editing.

a number of $n_x = 10$ elements in longitudinal direction of the accumulator is a good compromise between model complexity and accuracy. A further increase of n_x is not meaningful because the improvements that can be achieved are marginal. The same reasoning yields the choice $n_y = 3$ of elements in radial direction of the accumulator. Another important point for the simulation studies is the choice of the initial conditions. The initial gas pressure is set to the measured pressure. The initial piston temperature T_p is set to the oil temperature and the initial temperature of the sealing end T_e is given by the average of the ambient and a calculated gas temperature, i.e., $T_e = (T_{a,m} + T_{g,c})/2$. This temperature $T_{g,c}$ is calculated by the real gas equation (22) and the knowledge of m_g. The initial values of the CFRP pipe temperatures of *Model I* are chosen as $\bar{T}_{c,1,j} = (1-\xi_j)T_{g,c}+\xi_j T_{o,m}$, $\bar{T}_{c,2,j} = (1-\xi_j)(T_{g,c}+T_{c,m})/2 + \xi_j T_{o,m}$, and $\bar{T}_{c,3,j} = (1-\xi_j)T_{c,m} + \xi_j T_{o,m}$, $j = 1,\ldots,10$, with ξ_j from (17) and the measured temperature at the outer surface of the pipe $T_{c,m}$. For the *Model II* $\bar{T}_{c,m,j} = (1-\xi_j)(T_{g,c}+T_{c,m})/2 + \xi_j T_{o,m}$ with $j = 1,\ldots,10$ is used as initial values. In *Model III*, the temperature $\bar{T}_c$ is set to the weighted average $\bar{T}_c = (T_{g,c}+T_{c,m})s_p/(2l) + T_{o,m}(l-s_p)/l$ of the gas and oil temperature depending on the piston position s_p at time $t = 0$.

Figure 5 shows a comparison of the gas pressure and gas temperature of the three models with the measured values. The gas temperatures are compared to the temperature $T_{g,c}$, which is more reliable than a measured gas temperature, because measurements are always afflicted with errors due to the sensor dynamics and the thermal coupling with the ambience. Therefore, this temperature is used as the reference for validation. The simulated pressure of *Model I*, depicted in Figure 5(a), shows a very good agreement with the measured pressure in the overall range of operation. The same results can be observed by comparing the simulated and the calculated gas temperatures, cf. Figure 5(c). The larger errors of *Model II* in comparison to *Model I*, shown in Figure 5(b) and Figure 5(d), show the influence of the temperature gradient in y-direction, which was neglected in *Model II*. As expected, the further simplification of the heat transport from the gas to the CFRP pipe, which leads to *Model III*, results in even larger errors. In phases of high dynamics, the benefit of the longitudinal discretisation of *Model I* and *Model II* can be observed in the pressure and temperature errors. The root mean square values of the gas pressure error calculated over the whole measurement results is 2.91 bar for *Model I*, 3.31 bar for *Model II* and 5.26 bar for *Model III*. In general, the simplified models show higher errors at larger piston strokes. Figure 6 shows the pressure rms errors for different ranges of the piston position. Values below 50 % and above 90 % are left out because of the lack of measured data points. The presented results indicate a trend of higher accuracy at higher piston strokes. There is an influence of the degree of simplification of the CFRP-pipe models on the computation time: *Model II* can be simulated approximately 2.1 times faster than *Model I*, while the computation time for *Model III* is even a little bit faster but in the same range as *Model II*. Thus *Model I* is preferable for simulation studies, and *Model II* seems to be a good compromise between accuracy and numerical complexity for observer or controller design.

In Figure 7(a), the simulated temperatures of the piston are depicted. As it is expected, the large heat capacity of the solid piston inhibits fast variations of the temperature, e.g., in comparison to the gas temperature. Finally, Figure 7(b) gives the results for the measured surface temperature of the CFRP pipe at the fourth element of the CFRP pipe model of *Model I* and *Model II*, respectively. The simulated CFRP temperature is in good accordance with the measured CFRP temperature.

Post-print version of the article: A. Pfeffer, T. Glueck, W. Kemmetmueller, and A. Kugi, "Mathematical modelling of a hydraulic accumulator for hydraulic hybrid drives", *Mathematical and Computer Modelling of Dynamical Systems*, 2016. DOI: 10.1080/13873954.2016.1174716
The content of this post-print version is identical to the published paper but without the publisher's final layout or copy editing.

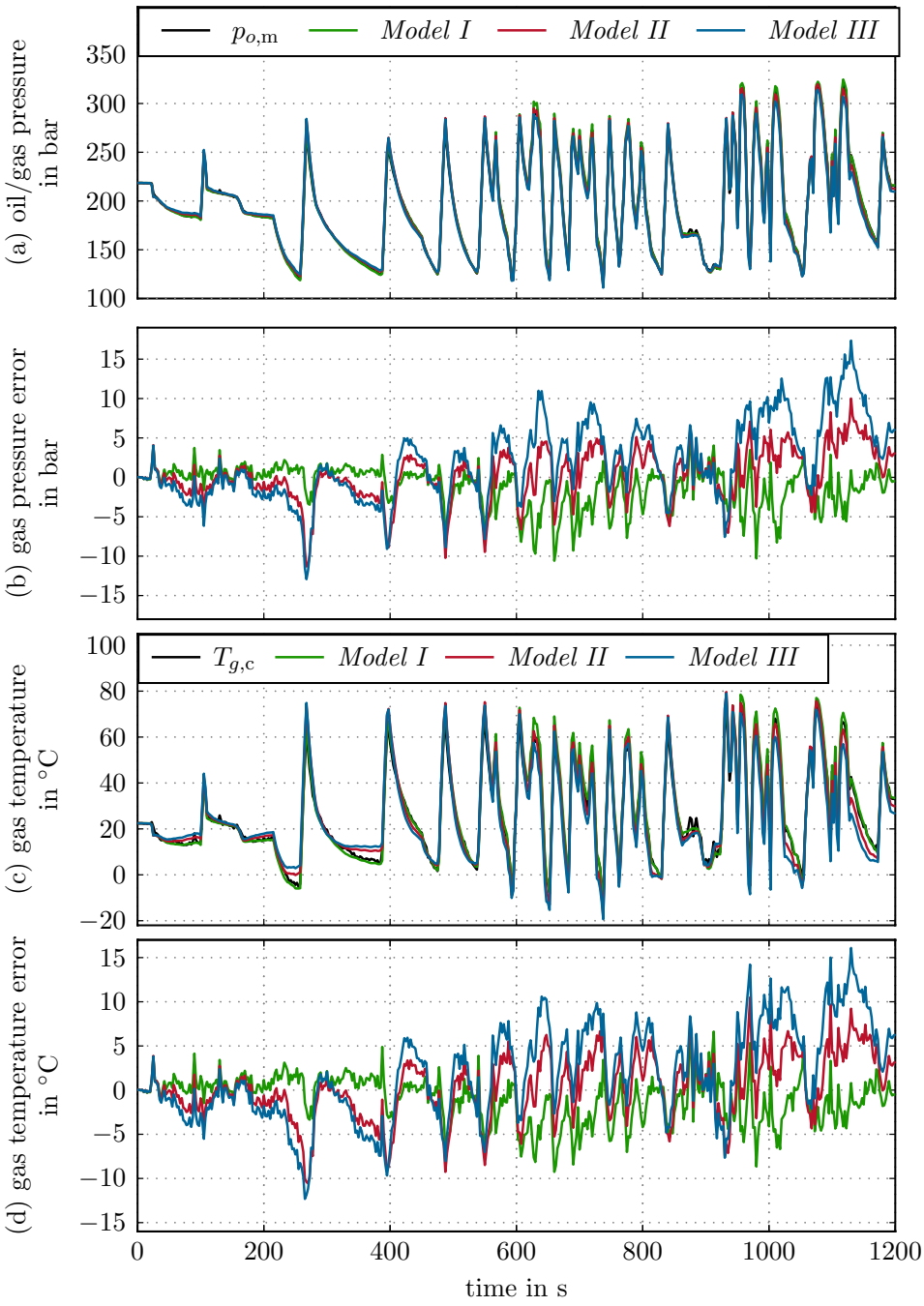

Figure 5. Comparison of the simulated model and measurement results: (a) measured oil pressure $p_{o,m}$ and simulated gas pressures; (b) errors between the measured and the simulated pressures; (c) calculated gas temperature $T_{g,\mathrm{c}}$ based on the measured piston position and the measured oil pressure, and the modelled gas temperatures; (d) error between the temperature $T_{g,c}$ and the modelled gas temperatures.

4. Conclusions

In this work, a detailed mathematical model for a hydraulic accumulator as a part of a hydraulic hybrid drive-train, taking into account the radial and axial temperature variation, was presented. The simulation results show a good agreement with measurements of the real system. Furthermore, two reduced models with respect

Post-print version of the article: A. Pfeffer, T. Glueck, W. Kemmetmueller, and A. Kugi, "Mathematical modelling of a hydraulic accumulator for hydraulic hybrid drives", *Mathematical and Computer Modelling of Dynamical Systems*, 2016. DOI: 10.1080/13873954.2016.1174716
The content of this post-print version is identical to the published paper but without the publisher's final layout or copy editing.

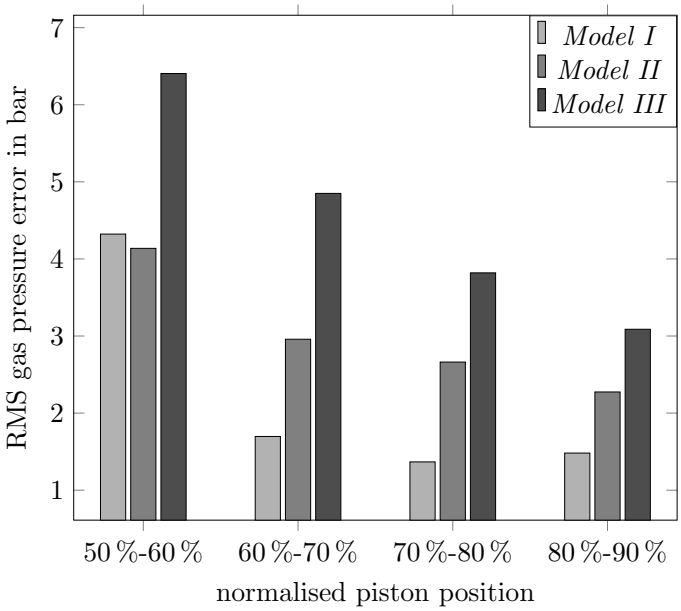

Figure 6. Comparison of the gas pressure root mean square errors of the three models in different piston position ranges.

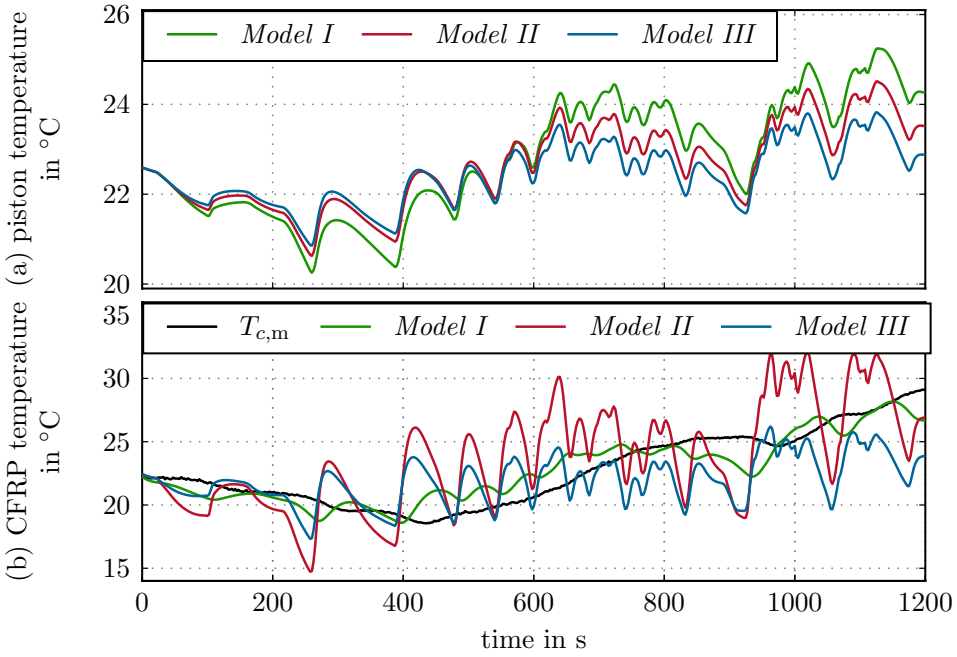

Figure 7. Comparison of the simulated model and measurement results: (a) modelled piston temperatures; (b) measured temperature on the outer surface of the CFRP pipe $T_{c,\mathrm{m}}$ and corresponding modelled temperatures $\bar{T}_{c,n_y,4}$ of *Model I*, $\bar{T}_{c,m,4}$ of *Model II* and $\bar{T}_c$ of *Model III*.

to the discretisation of the CFRP pipe in radial and axial directions have been proposed. The presented results show the high influence of these discretisations. While the impact of the radial discretisation is mainly recognisable at high piston strokes, the longitudinal discretisation is generally necessary for high model accuracy.

The presented model is intended as a basis for the design of estimator and controller strategies for hydraulic drive systems. Of course, this model can also be ap-

Post-print version of the article: A. Pfeffer, T. Glueck, W. Kemmetmueller, and A. Kugi, "Mathematical modelling of a hydraulic accumulator for hydraulic hybrid drives", *Mathematical and Computer Modelling of Dynamical Systems*, 2016. DOI: 10.1080/13873954.2016.1174716
The content of this post-print version is identical to the published paper but without the publisher's final layout or copy editing.

plied to other applications of piston type accumulators, e.g., [16, 17, 39]. Moreover, a transfer of the basic modelling approach to bladder type hydraulic accumulators is possible without great effort.

Acknowledgements

The authors thank Robert Bosch GmbH for funding this project. In particular, the authors highly appreciate the support of Adrian Trachte and Daniel Seiler-Thull.

References

[1] P. Soltic and L. Guzzella, *Verbrauchsvergleich verschiedener Verbrennungsmotorkonzepte für Leichtfahrzeuge*, MTZ - Motortechnische Zeitschrift 62 (2001), pp. 590–596.

[2] C. Chan, *The state of the art of electric, hybrid, and fuel cell vehicles*, Proceedings of the IEEE 95 (2007), pp. 704–718.

[3] G. Maggetto and J. Van Mierlo, *Electric and electric hybrid vehicle technology: a survey*, in *Electric, Hybrid and Fuel Cell Vehicles (Ref. No. 2000/050), IEE Seminar*, 11 April, Durham, UK, 2000.

[4] M.K. Yoong, Y.H. Gan, G.D. Gan, C.K. Leong, Z.Y. Phuan, B.K. Cheah, and K.W. Chew, *Studies of regenerative braking in electric vehicle*, in *Proceedings of IEEE Conference on Sustainable Utilization and Development in Engineering and Technology*, 20-21 Nov., Petaling Jaya, Malaysia, 2010, pp. 40–45.

[5] P. Thiebes, *Hybridantriebe für mobile Arbeitsmaschinen*, Ph.D. thesis, Karlsruher Institute of Technology, Karlsruhe, Germany, 2011.

[6] S. Wohlgemuth and G. Wachtmeister, *Hydropneumatic Storage Technology for Hybrid Passenger Cars*, in *3rd International Electric Drives Production Conference (EDPC) 2013*, 29 - 30 Oct., IEEE Catalog Number: CFP1385P-PRT, Nuremberg, Germany, 2013.

[7] A. Pourmovahed, N. Beachley, and F. Fronczak, *Modeling of a Hydraulic Energy Regeneration System: Part I–Analytical Treatment*, Journal of Dynamic Systems, Measurement and Control 114 (1992), pp. 155–159.

[8] A. Pourmovahed, N. Beachley, and F. Fronczak, *Modeling of a Hydraulic Energy Regeneration System: Part II–Experimental Program*, Journal of Dynamic Systems, Measurement and Control 114 (1992), pp. 160–165.

[9] T.H. Ho and K.K. Ahn, *Design and control of a closed-loop hydraulic energy-regenerative system*, Automation in Construction 22 (2012), pp. 444 – 458.

[10] R. Johri and Z. Filipi, *Low-cost pathway to ultra efficient city car: Series hydraulic hybrid system with optimized supervisory control*, SAE Int. J. Engines 2 (2009), pp. 505–520.

[11] T.O. Deppen, A. Alleyne, K.A. Stelson, and J.J. Meyer, *Optimal energy use in a light weight hydraulic hybrid passenger vehicle*, Journal of Dynamic Systems, Measurement and Control 134 (2012), pp. 041009–1 – 041009–11.

[12] K.L. Cheong, P. Li, and T. Chase, *Optimal design of power-split transmissions for hydraulic hybrid passenger vehicles*, in *Proceedings of the American Control Conference (ACC)*, 29 June - 1 July, San Francisco, CA, 2011, pp. 3295–3300.

[13] T.O. Deppen, A. Alleyne, J.J. Meyer, and K.A. Stelson, *Comparative study of energy management strategies for hydraulic hybrids*, Journal of Dynamic Systems, Measurement and Control 137 (2015), pp. 041002–1 – 041002–11.

[14] L.S. Louca and B.U. Yildir, *Modelling and reduction techniques for studies of integrated hybrid vehicle systems*, Mathematical and Computer Modelling of Dynamical Systems 12 (2006), pp. 203–218.

Post-print version of the article: A. Pfeffer, T. Glueck, W. Kemmetmueller, and A. Kugi, "Mathematical modelling of a hydraulic accumulator for hydraulic hybrid drives", *Mathematical and Computer Modelling of Dynamical Systems*, 2016. DOI: 10.1080/13873954.2016.1174716
The content of this post-print version is identical to the published paper but without the publisher's final layout or copy editing.

[15] T. Liu, J. Jiang, and H. Sun, *Investigation to Simulation of Regenerative Braking for Parallel Hydraulic Hybrid Vehicles*, in *Proceedings of the International Conference on Measuring Technology and Mechatronics Automation, 2009. ICMTMA '09.*, Vol. 2, 11-12 April, Zhangjiajie, Hunan, China, 2009, pp. 242–245.

[16] A. Oustaloup, B. Mathieu, and P. Lanusse, *The CRONE control of resonant plants: Application to a flexible transmission*, European Journal of Control 1 (1995), pp. 113 – 121.

[17] S. Lemofouet and A. Rufer, *A hybrid energy storage system based on compressed air and supercapacitors with maximum efficiency point tracking (MEPT)*, IEEE Transactions on Industrial Electronics 53 (2006), pp. 1105–1115.

[18] R. Dutta, F. Wang, B.F. Bohlmann, and K.A. Stelson, *Analysis of short-term energy storage for midsize hydrostatic wind turbine*, Journal of Dynamic Systems, Measurement and Control 136 (2014), pp. 011007–1 – 011007–9.

[19] S. Rotthäuser, *Verfahren zur Berechnung und Untersuchung hydropneumatischer Speicher*, Ph.D. thesis, RWTH Aachen, Aachen, Deutschland, 1993.

[20] H. Sedighnejad, T. Iqbal, and J. Quaicoe, *Performance evaluation of a hybrid wind-diesel-compressed air energy storage system*, in *Proceedings of the 24th Canadian Conference on Electrical and Computer Engineering (CCECE)*, 8-11 May, Niagara Falls, Canada, 2011, pp. 270–273.

[21] B. Manhartsgruber, G. Mikota, and R. Scheidl, *Modelling of a Switching Control Hydraulic System*, Mathematical and Computer Modelling of Dynamical Systems 11 (2005), pp. 329–344.

[22] Z. Filipi, L. Louca, B. Daran, C.C. Lin, U. Yildir, B. Wu, M. Kokkolaras, D. Assanis, H. Peng, P. Papalambros, J. Stein, D. Szkubiel, and R. Chapp, *Combined optimisation of design and power management of the hydraulic hybrid propulsion system for the 6 – 6 medium truck*, International Journal of Heavy Vehicle Systems 11 (2004), pp. 372–402.

[23] B. Wu, C.C. Lin, Z. Filipi, H. Peng, and D. Assanis, *Optimal power management for a hydraulic hybrid delivery truck*, Vehicle System Dynamics 42 (2004), pp. 23–40.

[24] M. Kaszynski and O. Sawodny, *Determining the fuel savings potential of parallel hybrid hydraulic vehicles*, International Journal of Powertrains 1 (2011), pp. 22–42.

[25] C.T. Li and H. Peng, *Optimal configuration design for hydraulic split hybrid vehicles*, in *Proceedings of the American Control Conference (ACC)*, 30 June - 2 July, Baltimore, MD, USA, 2010, pp. 5812–5817.

[26] A. Pfeffer, T. Glück, and W. Kemmetmüller, *State of Charge Estimator Design for a Gas Charged Hydraulic Accumulator*, Journal of Dynamic Systems, Measurement, and Control 137 (2015), pp. 061014–1 – 061014–9.

[27] A. Pourmovahed and D. Otis, *An experimental thermal time-constant correlation for hydraulic accumulators*, Journal of Dynamic Systems, Measurement and Control 112 (1990), pp. 116–121.

[28] D.R. Otis and A. Pourmovahed, *An Algorithm for Computing Nonflow Gas Processes in Gas Springs and Hydropneumatic Accumulators*, Journal of Dynamic Systems, Measurement, and Control 107 (1985), pp. 93–96.

[29] P. Puddu and M. Paderi, *Hydro-pneumatic accumulators for vehicles kinetic energy storage: Influence of gas compressibility and thermal losses on storage capability*, Energy 57 (2013), pp. 326 – 335.

[30] F. Tavares, R. Johri, and Z. Filipi, *Simulation Study of Advanced Variable Displacement Engine Coupled to Power-Split Hydraulic Hybrid Powertrain*, Journal of Engineering for Gas Turbines and Power 133 (2011), pp. 122803–1 – 122803–12.

[31] F.P. Incropera, D.P. Dewitt, T.L. Bergman, and A.S. Lavine, *Foundations of heat transfer*, 6th ed., John Wiley & Sons, Singapore, 2013.

[32] V.V. Sychev, *The Differential Equations of Thermodynamics*, 2nd ed., Hemisphere Publishing Corporation and Mir Publishers, New York and Moscow, 1991.

[33] R. Span, E.W. Lemmon, R.T. Jacobsen, W. Wagner, and A. Yokozeki, *A reference equation of state for the thermodynamic properties of nitrogen for temperatures from 63.151 to 1000 K and pressures to 2200 MPa*, J. Phys. Chem. Ref. Data 29 (2000),

Post-print version of the article: A. Pfeffer, T. Glueck, W. Kemmetmueller, and A. Kugi, "Mathematical modelling of a hydraulic accumulator for hydraulic hybrid drives", *Mathematical and Computer Modelling of Dynamical Systems*, 2016. DOI: 10.1080/13873954.2016.1174716
The content of this post-print version is identical to the published paper but without the publisher's final layout or copy editing.

pp. 1361–1433.
[34] VDI-Gesellschaft, *VDI Heat Atlas*, 2nd ed., Springer, Berlin, Heidelberg, 2010.
[35] K. Stephan and R. Krauss, *Viscosity and thermal conductivity of nitrogen for a wide range of fluid states*, Journal of Physical and Chemical Reference Data 16 (1987), pp. 993–1023.
[36] G. Gesellschaft and V.G.V.U. Chemieingenieurwesen, *VDI-Wärmeatlas: Berechnungsunterlagen für Druckverlust, Wärme- und Stoffübergang*, no. 1 in VDI-Buch Series, Springer, Berlin, Heidelberg, 2006.
[37] Electronic Sensor GmbH, Heilbronn, Germany, *Mineral insulated sheat-thermocouples* (2015), http://www.electronic-sensor.de/attachments/article/198/ti-3e_sheating-thermocouples.pdf, http://www.electronic-sensor.de/attachments/article/196/ti-1e_thermocouple-of-iec-584-3.pdf, access: 10.11.2015.
[38] Robert Bosch GmbH, Gerlingen-Schillerhöhe, Germany, *Technical Customer Information: DS-HD-KV4.2-TF*.
[39] P. Thiebes and M. Geimer, *Energy storage devices for industrial vehicles with hybrid drive trains*, in *VDI Fachkonferenz: "Getriebe in mobilen Arbeitsmaschinen" in Friedrichshafen*, VDI, Friedrichshafen, Germany, 2011.

Post-print version of the article: A. Pfeffer, T. Glueck, W. Kemmetmueller, and A. Kugi, "Mathematical modelling of a hydraulic accumulator for hydraulic hybrid drives", *Mathematical and Computer Modelling of Dynamical Systems*, 2016. DOI: 10.1080/13873954.2016.1174716
The content of this post-print version is identical to the published paper but without the publisher's final layout or copy editing.